Analysis and Reshaping on Impedance Characteristic of DFIG System based on Symmetrical PLL

Nian, Heng; Hu, Bin; Wu, Chao; Xu, Yunyang; Blaabjerg, Frede

Published in:
I E E E Transactions on Power Electronics

DOI (link to publication from Publisher):
10.1109/TPEL.2020.2982946

Publication date:
2020

Document Version
Accepted author manuscript, peer reviewed version

Analysis and Reshaping on Impedance Characteristic of DFIG System based on Symmetrical PLL

Heng Nian, *Senior Member, IEEE,* Bin Hu, Chao Wu, Liang Chen, Yunyang Xu, Frede Blaabjerg, *Fellow, IEEE*

***Abstract*—With the increasing penetration of renewable energy, wind turbines based on doubly fed induction generators (DFIG) are becoming more and more important in the power system. The impedance reshaping control strategy based on the virtual impedance method can be utilized to solve the stability problem of DFIG-grid interconnected system under the weak grid. However, the stability issues caused by phase locked loop (PLL) is more complicated due to the frequency coupling characteristic. This paper presents an improved control strategy of DFIG system based on a symmetrical PLL, in which the frequency coupling characteristic can be avoided and the system can be simplified as a SISO system that facilitates the design of virtual impedance. The influence of symmetrical PLL on the operation of DFIG system is studied, and an improved impedance reshaping control strategy is proposed. Simulation and experimental results are conducted to verify the effectiveness of the proposed impedance reshaping control strategy.**

***Index Terms*— Doubly-fed induction generator, symmetrical phase locked loop, frequency coupling, impedance reshaping control strategy.**

I. INTRODUCTION

Recently, with the increasing penetration of renewable energy, the installed capacity of wind power system continues to increase [1]. The wind power system based on doubly fed induction generator (DFIG) has been widely employed in practice, due to the advantages of small converter capacity, low cost and flexible power adjustment capability [2], [3].

Wind farms are usually built in remote areas such as offshore or in mountainous regions, indicating that the wind farm is always connected to the inductive weak grid with low short circuit ratio (SCR) [4]. The interaction between DFIG system and weak grid may cause some stability or resonance issues due to insufficient phase margin of the interconnected system [5]-[11]. Thus, there is great importance in analyzing stability issues of DFIG system connected to the weak grid for practical applications.

An effective method to solve the stability problem is to establish an impedance model of DFIG system and add the virtual impedance in the DFIG control [12]-[15]. The virtual impedance is composed of two parts, one is the filter to select the frequency range for impedance reshaping, and the other is the phase compensation controller to improve the phase margin of the DFIG system by regulating the phase characteristics around the oscillation frequency [16], [17]. The problem of sub-synchronous resonance and high frequency resonance has been investigated based on virtual impedance method [18], [19]. In [18], the virtual impedance controller is designed in both rotor-side and grid-side converters to eliminate sub-synchronous resonance. In [19], the high frequency resonance damping control and harmonic current suppression can be achieved simultaneously based on the proposed impedance reshaping control strategy.

In practice, the phase locked loop (PLL) is widely utilized to obtain the grid angle for implementing the grid synchronization. It has been reported that if the bandwidth of the PLL is too large, the PLL will influence phase characteristics of DFIG impedance within the bandwidth of the PLL, which bring a significant impact on the stability of DFIG-grid interconnected system especially under the weak grid conditions [5], [6]. However, reducing the bandwidth of the PLL will degrade the dynamic performance of the DFIG system, especially under asymmetric voltage faults [9]. Thus, it is significant to investigate the virtual impedance within the bandwidth of the PLL to reshape the phase characteristics, so that the dynamic performance of PLL cannot be affected.

A virtual impedance to compensate the impedance phase at the desired frequency is proposed for grid-connected inverters within the control bandwidth of the PLL in [20]. However, the strategy proposed in [20] neglects the frequency coupling characteristic caused by the PLL. Due to that the traditional PLL will introduce frequency coupling characteristics [9]-[11], the DFIG system impedance will become a multiple-input multiple-output (MIMO) matrix, and the design of virtual impedance within the control bandwidth of the PLL will be more difficult. Therefore, in order to improve the stability of DFIG system and to achieve an impedance reshaping of DFIG system, it is necessary to design four elements of virtual impedance, which increases the complexity of impedance reshaping.

To facilitate the analysis of the impedance model, some researchers have studied the mathematical methods to approximate the MIMO system to the single-input single-output (SISO) system [21], [22]. However, all mathematical methods transform the off-diagonal elements of the DFIG system to diagonal based on linear transformation, which does not really remove the frequency coupling characteristics. Aimed at this question, [23] proposed a symmetrical PLL, which controls both *d*-axis voltage and *q*-axis voltage. The frequency coupling characteristics can be eliminated so that the design of the impedance reshaping parameters can be simplified.

In order to enhance the stability of DFIG system connected to weak grid, the improved control strategy of DFIG system based on symmetrical PLL is proposed in this paper. The simplified SISO impedance model of DFIG system based on the symmetrical PLL is established firstly, which can eliminate the frequency coupling caused by the traditional PLL. Then, the influence of symmetrical PLL on DFIG is studied, and an

This article has been accepted for publication in a future issue of this journal, but has not been fully edited. Content may change prior to final publication. Citation information: DOI 10.1109/TPEL.2020.2982946, IEEE Transactions on Power Electronics

improved impedance reshaping control strategy is proposed by improving the phase margin within the control bandwidth of the symmetrical PLL. It is also convenient to design the parameters of virtual impedance based on the simplified SISO impedance model.

This paper is organized as follows. Section II describes the DFIG system configuration based on symmetrical PLL. The impedance model of DFIG based on symmetrical PLL is developed in Section III. Section IV validates and analyzes the proposed impedance model, then the impedance reshaping control strategy is introduced in Section V. Section VI gives the experiment results to verify the effectiveness of the proposed impedance reshaping control strategy. Section VII draws the conclusion.

II. DFIG System Configuration with sSmmetrical PLL

Considering that the back-to-back converter of the DFIG system is composed of the rotor side converter (RSC) and grid side converter (GSC), the DFIG is always controlled by the RSC to achieve maximum power point tracking (MPPT), while the dc voltage is controlled to be constant by the GSC. Therefore, the overall output impedance of DFIG system is equivalent to the parallel connection of DFIG+RSC and GSC. Since the impedance amplitude of GSC is greater than the DFIG+RSC within the bandwidth of the PLL [11], it becomes widely accepted that GSC has less impact on impedance than DFIG+RSC within the bandwidth of the PLL. Thus, only the impedance of DFIG+RSC is analyzed in this paper.

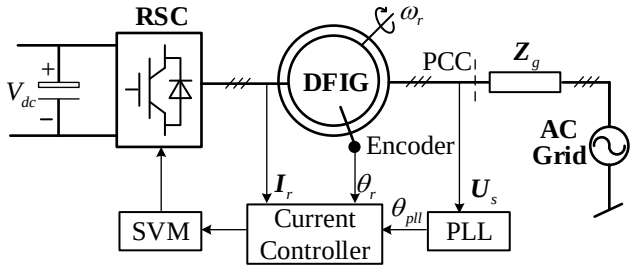

Fig. 1. Topology of DFIG connected to three phase AC grid.

The topology of DFIG+RSC can be seen as Fig. 1. The bold letters are used in this paper to denote complex space vectors or 2×2 matrix. The dc-link voltage V_{dc} is assumed to be constant. $\boldsymbol{Z}_g$ is the grid impedance. The stator voltage $\boldsymbol{U}_s$ is sampled from point of common coupling (PCC). The rotor angular frequency ω_r and rotor angle θ_r are obtained by an encoder. Grid angle θ_{pll} and drive signals are obtained by PLL and rotor current controller.

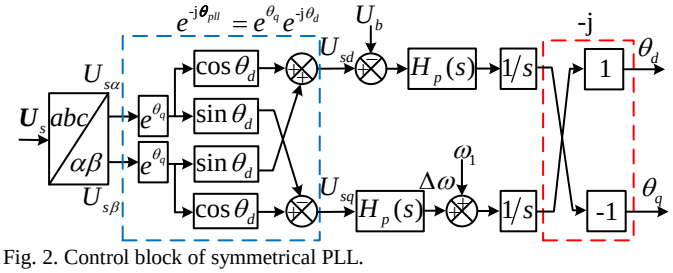

Fig. 2. Control block of symmetrical PLL.

Fig. 2 shows the control block of a symmetrical PLL [23]. The subscripts α and β represent the component in the two-phase stationary coordinate system. The subscripts d and q represent the component in the synchronous rotating coordinate system, respectively. ω_1 is the fundamental angular frequency of grid voltage. $H_p(s)=K_{pp}+K_{ip}/s$ is PI controller of the PLL, in which K_{pp} and K_{ip} are the proportional and the integral gains of PLL.

The conventional SRF-PLL only controls the q-axis voltage, which results in asymmetric dynamics to the d- and q-axis controller. Different from conventional SRF-PLL, symmetrical PLL controls both d-axis voltage and q-axis voltage, in which the nominal value U_b of grid voltage is taken as a reference for d-axis voltage control. The output grid angle of the symmetrical PLL is a complex vector, which includes both d-axis and q-axis components, i.e., $\boldsymbol{\theta}_{pll}=\theta_d+\mathrm{j}\theta_q$. The grid vector angle $\boldsymbol{\theta}_{pll}$ will be used for the coordinate transformation of voltage and current.

III. Impedance Modeling of DFIG based on Symmetrical PLL

In order to study the stability of DFIG system based on the symmetrical PLL in the inductive weak grid, it is necessary to establish the dq-domain impedance model firstly. Through the transformation matrix between dq-domain and sequence-domain, the sequence impedance model of DFIG system based on symmetrical PLL can be obtained.

A. Sequence-Domain Model of DFIG

The voltage and flux linkages in stationary coordinate system can be expressed as,

$$\begin{cases} \boldsymbol{U}_s = R_s\boldsymbol{I}_s + s\boldsymbol{\psi}_s \\ \boldsymbol{U}_r = R_r\boldsymbol{I}_r + s\boldsymbol{\psi}_r - j\omega_r\boldsymbol{\psi}_r \end{cases} \tag{1}$$

$$\begin{cases} \boldsymbol{\psi}_s = L_s\boldsymbol{I}_s + L_m\boldsymbol{I}_r \\ \boldsymbol{\psi}_r = L_m\boldsymbol{I}_s + L_r\boldsymbol{I}_r \end{cases} \tag{2}$$

where U, I and Ψ denote the voltage, current and the flux linkage, respectively. The subscripts s and r denote the stator and rotor parameters. R_s and R_r are stator and rotor resistances, $L_m=1.5L_{ms}$, $L_s=1.5L_{ms}+L_{ls}$ and $L_r=1.5L_{ms}+L_{lr}$ are self-inductance of stator and rotor windings, L_{ls}, L_{lr}, L_{ms} are stator and rotor leakage inductances and mutual inductance, respectively.

Based on (2), the rotor flux linkage can be expressed in the terms of stator flux linkage and rotor current as,

$$\boldsymbol{\psi}_r = \frac{L_m}{L_s}\boldsymbol{\psi}_s + L_r\sigma\boldsymbol{I}_r \tag{3}$$

where $\sigma=1-L_m^2/(L_s\cdot L_r)$.

Submitting (3) into (1), the rotor voltage can be rewritten as,

$$\boldsymbol{U}_r = \left[R_r+\left(s-j\omega_r\right)L_r\sigma\right]\boldsymbol{I}_r + \left(s-\mathrm{j}\omega_r\right)\frac{L_m}{L_s}\boldsymbol{\psi}_s \tag{4}$$

Ignoring the stator resistance and combining (1), (3), (4) to eliminate rotor current and stator flux linkage, the positive and negative sequence-domain equation of DFIG are expressed as,

$$\begin{bmatrix} I_{sp} \\ I_{sn} \end{bmatrix} = \left(\frac{1}{L_s}\boldsymbol{G}_1 + \frac{L_m}{L_s}\boldsymbol{G}_1\boldsymbol{G}_2\boldsymbol{G}_3\right)\begin{bmatrix} U_{sp} \\ U_{sn} \end{bmatrix} - \frac{L_m}{L_s}\boldsymbol{G}_3\begin{bmatrix} U_{rp} \\ U_{rn} \end{bmatrix} \tag{5}$$

This article has been accepted for publication in a future issue of this journal, but has not been fully edited. Content may change prior to final publication. Citation information: DOI 10.1109/TPEL.2020.2982946, IEEE Transactions on Power Electronics

$$\boldsymbol{G}_1=\begin{bmatrix}\dfrac{1}{s} & 0\\ 0 & \dfrac{1}{s-2\mathrm{j}\omega_1}\end{bmatrix}\quad \boldsymbol{G}_2=\frac{L_m}{L_s}\begin{bmatrix}s-\mathrm{j}\omega_r & 0\\ 0 & s+\mathrm{j}\omega_r-2\mathrm{j}\omega_1\end{bmatrix}$$
$$\boldsymbol{G}_3=\begin{bmatrix}\dfrac{1}{R_r+(s-\mathrm{j}\omega_r)L_r\sigma} & 0\\ 0 & \dfrac{1}{R_r+(s+\mathrm{j}\omega_r-2\mathrm{j}\omega_1)L_r\sigma}\end{bmatrix} \tag{6}$$

where subscripts *p* and *n* denote positive and negative sequence components. The positive and negative sequence subsystem are in opposite direction which differ by two times fundamental frequency $2\omega_1$, and the slip behaves as $\pm\omega_r$ because of the reversed turns in the positive sequence and negative sequence.

It can be found that the matrices $\boldsymbol{G}_1$, $\boldsymbol{G}_2$, and $\boldsymbol{G}_3$ are all diagonal matrices, so there is no frequency coupling characteristics of the DFIG when the RSC is not considered.

B. Small-Signal Model of RSC in dq-Domain

Compared with the symmetrical PLL in the grid-connected voltage-source converter in [23], the coordinate transformation of DFIG involves the rotor angle. Therefore, this paper will derive the small-signal model of the symmetrical PLL in DFIG.

There are two coordinate frames in DFIG system, one is the system frame, which is defined by the real grid voltage, and the other is the controller frame, which is defined by the PLL [12]. The steady-state components of stator voltage are the same in the system frame and the controller frame when there is no disturbance, i.e., $\boldsymbol{U}_{sdq}=\boldsymbol{U}^c_{sdq}=U_{sd1}$, in which superscript *c* denotes controller frame, subscript 1 denotes steady-state component. U_{sd1} is the steady-state stator voltage vector aligned to the *d*-axis, i.e., the steady-state stator voltage $\boldsymbol{U}_{sdq1}=U_{sd1}+\mathrm{j}0$.

The grid angle $\boldsymbol{\theta}_{pll}$ is obtained by PLL, which will be affected by the PCC voltage perturbations. The response of grid angle corresponding to the voltage perturbation can be expressed as,

$$\boldsymbol{\theta}_{pll}=\omega_1 t+\Delta\boldsymbol{\theta}_{pll} \tag{7}$$

And the grid angle $\boldsymbol{\theta}_{pll}$ is involved in the following two transformation links,

$$\boldsymbol{I}^c_{rdq}=e^{-\mathrm{j}(\boldsymbol{\theta}_{pll}-\theta_r)}\boldsymbol{I}_{r\alpha\beta}\qquad \boldsymbol{U}_{r\alpha\beta}=e^{\mathrm{j}(\boldsymbol{\theta}_{pll}-\theta_r)}\boldsymbol{U}^c_{rdq} \tag{8}$$

Given a perturbation on the PCC voltage in the *dq* frame, the small-signal component of stator voltage can be expressed as,

$$\begin{aligned}&U_{sd1}+\Delta\boldsymbol{U}^c_{sdq}=e^{-\mathrm{j}\boldsymbol{\theta}_{pll}}\boldsymbol{U}_{s\alpha\beta}=\left(U_{sd1}+\Delta\boldsymbol{U}_{sdq}\right)e^{-\mathrm{j}\Delta\boldsymbol{\theta}_{pll}}\\ &\approx\left(U_{sd1}+\Delta\boldsymbol{U}_{sdq}\right)\left(1-\mathrm{j}\Delta\boldsymbol{\theta}_{pll}\right)\Rightarrow\Delta\boldsymbol{U}^c_{sdq}=\Delta\boldsymbol{U}_{sdq}-\mathrm{j}U_{sd1}\Delta\boldsymbol{\theta}_{pll}\end{aligned} \tag{9}$$

Then, according to the structure of the symmetrical PLL, the relationship between the grid angle variation and the stator voltage variation can be expressed as,

$$\Delta\boldsymbol{\theta}_{pll}=-\mathrm{j}\frac{H_p(s)}{s-\mathrm{j}\omega_1}\Delta\boldsymbol{U}^c_{sdq} \tag{10}$$

$$H_p(s)=\frac{K_{pp}(s-\mathrm{j}\omega_1)+K_{ip}}{s-\mathrm{j}\omega_1} \tag{11}$$

Substituting (9) into (10), the small-signal model of symmetrical PLL can be derived as,

$$\Delta\boldsymbol{\theta}_{pll}=-\mathrm{j}H_{pll}(s)\Delta\boldsymbol{U}_{sdq}=-\mathrm{j}\frac{H_p(s)}{U_{sd1}H_p(s)+s-\mathrm{j}\omega_1}\Delta\boldsymbol{U}_{sdq} \tag{12}$$

Similar to (9), the effect of voltage perturbations on rotor current and rotor voltage should also be analyzed. The park transformation of rotor current can be expressed as,

$$\boldsymbol{I}_{rdq1}+\Delta\boldsymbol{I}^c_{rdq}=e^{-\mathrm{j}(\boldsymbol{\theta}_{pll}-\theta_r)}\boldsymbol{I}_{r\alpha\beta}=\left(\boldsymbol{I}_{rdq1}+\Delta\boldsymbol{I}_{rdq}\right)e^{-\mathrm{j}\Delta\boldsymbol{\theta}_{pll}} \tag{13}$$

Thus, the influence of symmetrical PLL on rotor current can be expressed as,

$$\Delta\boldsymbol{I}^c_{rdq}=\Delta\boldsymbol{I}_{rdq}+\boldsymbol{G}_{dqi}\Delta\boldsymbol{U}_{sdq} \tag{14}$$

$$\boldsymbol{G}_{dqi}=\begin{bmatrix}-I_{rd1}H_{pll}(s) & I_{rq1}H_{pll}(s)\\ -I_{rq1}H_{pll}(s) & -I_{rd1}H_{pll}(s)\end{bmatrix} \tag{15}$$

Likewise, the influence of symmetrical PLL on rotor voltage can be expressed as,

$$\Delta\boldsymbol{U}_{rdq}=\Delta\boldsymbol{U}^c_{rdq}+\boldsymbol{G}_{dqu}\Delta\boldsymbol{U}_{sdq} \tag{16}$$

$$\boldsymbol{G}_{dqu}=\begin{bmatrix}U_{rd1}H_{pll}(s) & -U_{rq1}H_{pll}(s)\\ U_{rq1}H_{pll}(s) & U_{rd1}H_{pll}(s)\end{bmatrix} \tag{17}$$

C. Small-Signal Model of RSC in Sequence- Domain

The sequence impedance has a clear physical meaning and it is easier to measure directly than the *dq*-domain impedance [14]. Therefore, in order to study the frequency characteristics of DFIG system based on symmetrical PLL more intuitively, this paper transforms the *dq*-domain small-signal model into the sequence-domain small-signal model. According to [13], the transformation matrix can be expressed as,

$$\begin{cases}\boldsymbol{G}_{pni}=\boldsymbol{A}_z\boldsymbol{G}_{dqi}\boldsymbol{A}_z^{-1}\\ \boldsymbol{G}_{pnu}=\boldsymbol{A}_z\boldsymbol{G}_{dqu}\boldsymbol{A}_z^{-1}\end{cases} \tag{18}$$

$$\boldsymbol{A}_z=\frac{1}{\sqrt{2}}\begin{bmatrix}1 & \mathrm{j}\\ 1 & -\mathrm{j}\end{bmatrix}\qquad \boldsymbol{A}_z^{-1}=\frac{1}{\sqrt{2}}\begin{bmatrix}1 & 1\\ -\mathrm{j} & \mathrm{j}\end{bmatrix} \tag{19}$$

The stator voltage feedforward matrices due to the symmetrical PLL in the sequence-domain can be expressed as,

$$\boldsymbol{G}_{pni}=\begin{bmatrix}-\boldsymbol{I}_{rdq1}H_{pll}(s) & 0\\ 0 & -\boldsymbol{I}^*_{rdq1}H_{pll}(s)\end{bmatrix} \tag{20}$$

$$\boldsymbol{G}_{pnu}=\begin{bmatrix}\boldsymbol{U}_{rdq1}H_{pll}(s) & 0\\ 0 & \boldsymbol{U}^*_{rdq1}H_{pll}(s)\end{bmatrix} \tag{21}$$

where * denotes the conjugate operator.

When the diagonal elements of matrix are the same and the off-diagonal elements are opposite to each other, this is defined as the symmetrical matrix [23], i.e., the matrices in (15) and (17). After performing a linear transformation according to (18), it can be equivalently transformed into a SISO matrix, which only has the diagonal components, i.e., the stator voltage feedforward matrices $\boldsymbol{G}_{pni}$ and $\boldsymbol{G}_{pnu}$.

Since the SRF-PLL only controls the *q*-axis voltage, the stator voltage feedforward matrix in the *dq*-domain is not a symmetrical matrix, which introduces the MIMO matrix in sequence-domain after linear transformation. As a result, the

This article has been accepted for publication in a future issue of this journal, but has not been fully edited. Content may change prior to final publication. Citation information: DOI 10.1109/TPEL.2020.2982946, IEEE Transactions on Power Electronics

frequency coupling characteristics is inevitable due to SRF-PLL, which makes the impedance analysis complicated. When designing the virtual impedance to improve the stability of DFIG system, it is necessary to design four elements in diagonal and off-diagonal, which increases the complexity of impedance reshaping.

D. Impedance Model of DFIG System with Symmetrical PLL

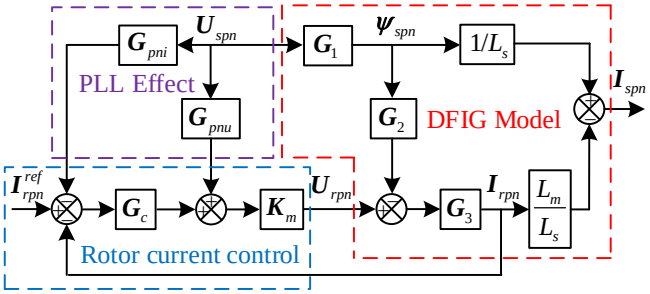

Fig. 3. DFIG impedance model based on symmetrical PLL.

According to (5), (14) and (16), the DFIG impedance model based on symmetrical PLL can be depicted by Fig. 3. $\boldsymbol{I}_{rpn}^{ref}$ is the reference value of rotor current, and the symbol "Δ" is omitted for simplicity. The stator current can be expressed as,

$$\boldsymbol{I}_{spn} = \boldsymbol{Y}_{\mathrm{DFIG}}\boldsymbol{U}_{spn} + \boldsymbol{I}_{rpn}^{ref}\boldsymbol{G}_{ref} \tag{22}$$

where $\boldsymbol{Y}_{\mathrm{DFIG}}$ represents the DFIG system admittance based on the symmetrical PLL, and $\boldsymbol{G}_{ref}$ describes the relationship between the rotor current and rotor current reference, that can be expressed as,

$$\begin{aligned}\boldsymbol{Y}_{\mathrm{DFIG}} &= \begin{bmatrix} Y_{11} & 0 \\ 0 & Y_{22} \end{bmatrix} = \frac{1}{L_s}\boldsymbol{G}_1 - \left(\boldsymbol{I} + \boldsymbol{K}_m\boldsymbol{G}_c\boldsymbol{G}_3\right)^{-1} \\ &\quad \frac{L_m}{L_s}\boldsymbol{G}_3\left(\boldsymbol{K}_m\boldsymbol{G}_{pnu} - \boldsymbol{K}_m\boldsymbol{G}_c\boldsymbol{G}_{pni} - \boldsymbol{G}_2\boldsymbol{G}_1\right)\end{aligned} \tag{23}$$

$$\boldsymbol{G}_{ref} = -\frac{L_m}{L_s}\left(\boldsymbol{I} + \boldsymbol{K}_m\boldsymbol{G}_c\boldsymbol{G}_3\right)^{-1}\boldsymbol{K}_m\boldsymbol{G}_c\boldsymbol{G}_3 \tag{24}$$

where $\boldsymbol{K}_m$ represents the system delay matrix, and the delay time is equal to 1.5 times the switching period T_s [11]. $\boldsymbol{G}_c$ is the rotor current controller matrix, K_{pc} and K_{ic} are the proportional and the integral gain of current controller. Noted that $\boldsymbol{G}_c$ keeps unchanged after transformation, i.e., $\boldsymbol{G}_c=\boldsymbol{A}_z\boldsymbol{G}_c\boldsymbol{A}_z^{-1}$, so the rotor current controller has the same form in *dq*-domain and sequence-domain.

$$\boldsymbol{K}_m = \begin{bmatrix} e^{-1.5T_s s} & 0 \\ 0 & e^{-1.5T_s(s-2j\omega_1)} \end{bmatrix} \tag{25}$$

$$\boldsymbol{G}_c = \begin{bmatrix} \dfrac{K_{pc}(s-\mathrm{j}\omega_1)+K_{ic}}{s-\mathrm{j}\omega_1} & 0 \\ 0 & \dfrac{K_{pc}(s-\mathrm{j}\omega_1)+K_{ic}}{s-\mathrm{j}\omega_1} \end{bmatrix} \tag{26}$$

All the matrices of DFIG system admittance are diagonal matrices, indicating that the DFIG system based on symmetrical PLL has no frequency coupling characteristics.

IV. Impedance Model Verification and Analysis

A. Impedance Model Verification

In order to verify the correctness of DFIG system impedance model based on symmetrical PLL, a simulation model of DFIG system is established in Matlab/Simulink. Frequency sweeping test is a widely applied method to obtain the system impedance results by measuring the frequency responses within a certain frequency range. The measured results and the developed models are plotted to be compared in Bode diagrams. The parameters are shown in Table I.

A comparison of DFIG system impedance model based on symmetrical PLL and simulation results as shown in Fig. 4. Noted that Fig. 4 depicts the Bode diagram of DFIG impedance rather than DFIG admittance to describe the impedance characteristics more intuitively. When the bandwidth of symmetrical PLL f_{bw_PLL} is 140 Hz, the analytical models of DFIG based on symmetrical PLL match the simulations well, thus the accuracy of the analytical models can be validated. In addition, other working conditions of DFIG such as sub-synchronous conditions are also be validated which not appear in this paper due to the limited pages.

TABLE I
PARAMETER OF DFIG

Symbol	Parameter	Value
U_s	Rated voltage	690 V
P_s	Rated power	1.5 MW
f_1	Fundamental frequency	50 Hz
f_r	Rotor frequency	60 Hz
n_p	Pole pairs	2
V_{dc}	Dc-link voltage	1050 V
L_{ls}	Stator leakage	0.06 mH
L_{lr}	Rotor leakage	0.083 mH
L_{ms}	Mutual inductance	2.95 mH
R_s	Stator resistance	2.4 mΩ
R_r	Rotor resistance	2 mΩ
K_e	Turns ratio	0.33
T_s	Switching period	0.2 ms
K_{pp}	Proportional gain of PLL controller	1.6
K_{ip}	Integral gain of PLL controller	16
K_{pc}	Proportional gain of current controller	0.38
K_{ic}	Integral gain of current controller	38

If the impedance magnitude of the off-diagonal elements is high, the positive-sequence and negative-sequence will not affect each other due to a strong damping. By comparing the diagonal elements Z_{11} and Z_{22} with the off-diagonal elements Z_{12} and Z_{21}, it can be seen that the magnitude of diagonal elements is much smaller than the off-diagonal elements, which means the frequency coupling characteristics can be neglected, simplifying the difficulty of impedance model analysis.

A resonance frequency at almost 100 Hz will be observed in Z_{22}. Because 100 Hz of negative sequence corresponds to 0 Hz

This article has been accepted for publication in a future issue of this journal, but has not been fully edited. Content may change prior to final publication. Citation information: DOI 10.1109/TPEL.2020.2982946, IEEE Transactions on Power Electronics

of positive sequence, and the DFIG system cannot work with large DC interference. It is noted that when there is no frequency coupling, the negative sequence impedance can be neglected and the stability of DFIG system can be analyzed based on the Bode diagram of positive sequence impedance [10]. On the one hand, the negative sequence impedance from 0 Hz to 100 Hz corresponds to positive sequence impedance from 100 Hz to 0 Hz, which is redundancy in the impedance analysis. On the other hand, the phase of negative sequence impedance from 100 Hz to 1000 Hz is between -20° and 100° as shown in Fig 4. Therefore, the positive sequence impedance model is adopted in this paper.

It can be found that below the fundamental frequency, the DFIG behaves as a negative resistance. This phenomenon can be explained by the induction generator effect (IGE) and sub-synchronous control interaction (SSCI) [24], [25]. Within the control bandwidth of the symmetrical PLL, the phase characteristics of DFIG changes from negative resistance to capacitance, and finally to resistance. Above the current control bandwidth, the phase of the positive sequence impedance tends to be inductive. Since the control effect of controllers can be ignored in the high frequency range, the characteristics of DFIG system is dominated by its passive components.

The analytical model of Z_{11} and Z_{22} when f_{bw_PLL}=80 Hz is also drawn in Fig. 4, the amplitude-frequency characteristic curves of DFIG and grid both intersect at 136 Hz when f_{bw_PLL} is 80 Hz or 140 Hz. DFIG behaves as a capacitance at 136 Hz and the phase margin is less than 0° when f_{bw_PLL}=140 Hz, which means the DFIG-grid interconnected system is unstable. The resonance phenomenon of the DFIG is shown as Fig. 5, in which the DFIG-grid interconnected system becomes unstable when f_{bw_PLL} changes from 80 Hz to 140 Hz at 2.5s. The resonant frequency of the active power at 136 Hz can be predicted accurately as shown in Fig. 6 and there is no other coupling frequency based on FFT analysis of stator voltage. It is essential to study the cause of resonance and the virtual impedance will be introduced to suppress the resonance.

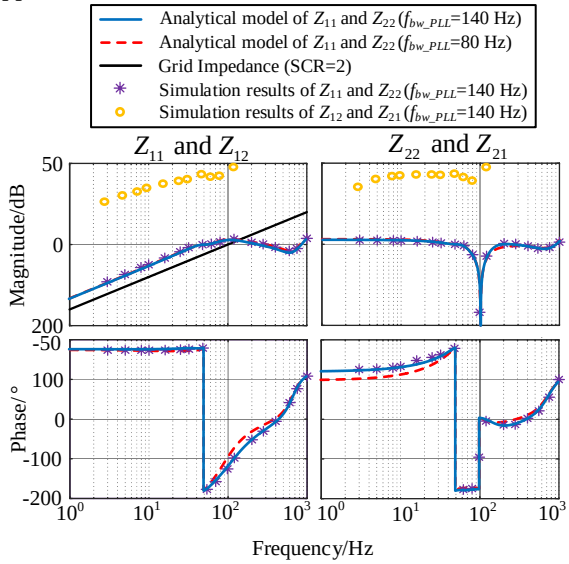

Fig. 4. Validation of DFIG impedance models based on symmetrical PLL.

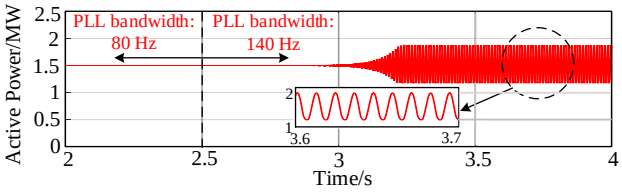

Fig. 5. Resonance phenomenon of DFIG based on symmetrical PLL (SCR=2).

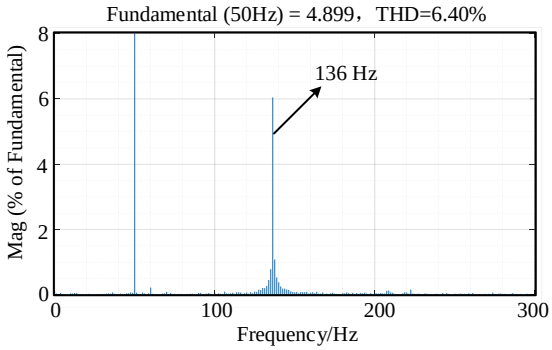

Fig. 6. FFT analysis of stator voltage.

B. *Impedance Model Analysis*

Based on the SISO impedance model, the resonance issues of DFIG-grid interconnected system will occur as the bandwidth of the symmetrical PLL increases. According to Fig. 3, symmetrical PLL will introduce two stator voltage feedforward matrices $\boldsymbol{G}_{pni}$ and $\boldsymbol{G}_{pnu}$, which will influence the impedance characteristics of DFIG system. To further analyze the influence factor and design the suitable virtual impedance, the impedance of DFIG needs to be decomposed into:

$$\boldsymbol{Z}_{\mathrm{DFIG}}=\left(1/\boldsymbol{Z}_0+1/\boldsymbol{Z}_{pnu}+1/\boldsymbol{Z}_{pni}\right)^{-1} \tag{27}$$

where $\boldsymbol{Z}_0$ is DFIG impedance, which ignores the symmetrical PLL, $\boldsymbol{Z}_{pnu}$ and $\boldsymbol{Z}_{pni}$ are the parallel impedance based on the symmetrical PLL due to coordinate transformation of rotor voltage and rotor current. Fig. 7 shows the block diagram of DFIG impedance subsystem.

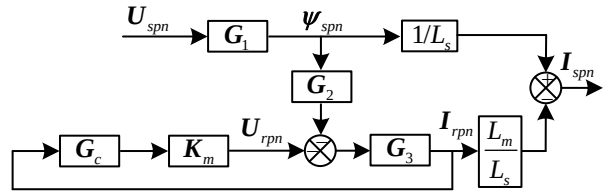

(a) $\boldsymbol{Z}_0$

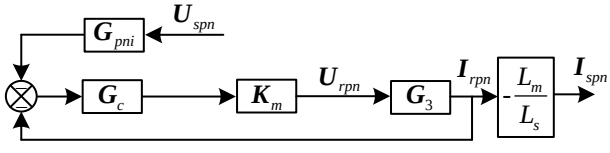

(b) $\boldsymbol{Z}_{pnu}$

This article has been accepted for publication in a future issue of this journal, but has not been fully edited. Content may change prior to final publication. Citation information: DOI 10.1109/TPEL.2020.2982946, IEEE Transactions on Power Electronics

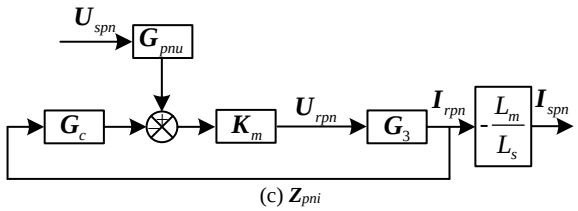

(c) $\boldsymbol{Z}_{pni}$

Fig. 7. Block diagram of DFIG impedance subsystem.

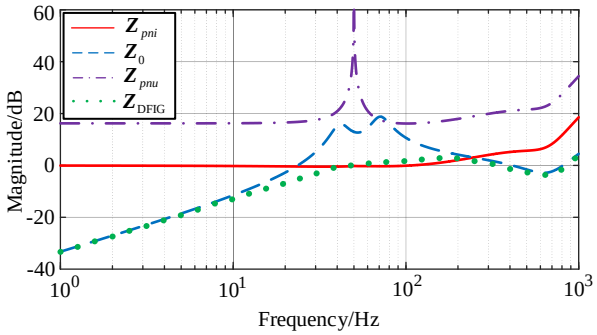

Fig. 8. Amplitude-frequency characteristic curves of impedance subsystem.

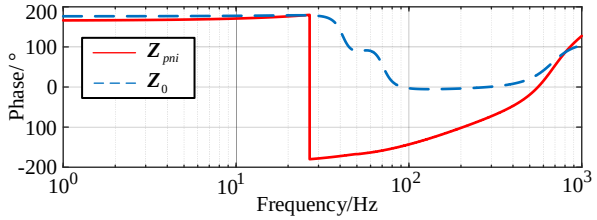

Fig. 9. Phase-frequency characteristic curves of DFIG impedance subsystem.

Fig. 8 and Fig. 9 depicts the amplitude-frequency characteristic curves and phase-frequency characteristic curves of DFIG impedance subsystem. From Fig. 8 and Fig. 9, several conclusions can be reached as follows.

Firstly, since the magnitude of parallel impedance $\boldsymbol{Z}_{pnu}$ is greater than 17 dB within the whole frequency range, $\boldsymbol{Z}_{pnu}$ can be neglected in the analysis of the DFIG impedance.

Secondly, the amplitude-frequency characteristic curves of $\boldsymbol{Z}_{\mathrm{DFIG}}$ is approximated to $\boldsymbol{Z}_0$ above 500 Hz or less than 10 Hz, where the control effect of the controllers can be ignored. The phase of $\boldsymbol{Z}_0$ is always between 0 ° and 180 °, therefore, the DFIG-grid interconnected system is always stable with the connection to the inductive weak grid when the effect of symmetrical PLL is ignored.

Thirdly, the amplitude-frequency characteristic curves of $\boldsymbol{Z}_{\mathrm{DFIG}}$ is approximated to $\boldsymbol{Z}_{pni}$ between 50 Hz and 200 Hz, thus $\boldsymbol{Z}_{pni}$ dominates the impedance characteristics of DFIG within this frequency range. $\boldsymbol{Z}_{pni}$ behaves as a negative resistance around the fundamental frequency, and becomes capacitive gradually as the frequency increases, which will cause a potential risk of resonance.

In conclusion, the resonance reason for the DFIG system lies in the fact that the symmetrical PLL will introduce the parallel impedance $\boldsymbol{Z}_{pni}$ when performing rotor current coordinate transformation. Therefore, it is necessary to derive the expression of $\boldsymbol{Z}_{pni}$.

C. *Impedance Analysis of $\boldsymbol{Z}_{pni}$*

Ignoring the system delay matrix $\boldsymbol{K}_m$ which always influences the impedance characteristics of high frequency, and approximately considering L_m/L_s=1, the equivalent expression of Z'_{pni} can be expressed as,

$$Z'_{pni} \approx \frac{1+G'_cG'_3}{G'_{pni}G'_cG'_3} = \frac{1/G'_3+G'_c}{G'_{pni}G'_c} \tag{28}$$

where the superscript $'$ denotes the first element in the first row of the matrix, which represents the transfer function between the positive sequence elements of stator voltage and stator current. The denominator of Z'_{pni} contains $1/G'_3$ and G'_c,

$$1/G'_3 = R_r + (s - \mathrm{j}\omega_r)L_r\sigma \tag{29}$$

$$G'_c = \frac{K_{pc}(s - \mathrm{j}\omega_1) + K_{ic}}{s - \mathrm{j}\omega_1} \tag{30}$$

It should be noted that $1/G'_3$ is much smaller than G'_c near the fundamental frequency. Therefore, $1/G'_3$ can be ignored and (28) can be expressed approximately as,

$$Z'_{pni} \approx \frac{1}{G'_{pni}} = -\frac{1}{\boldsymbol{I}_{rdq1}}\left(\frac{(s - \mathrm{j}\omega_1)^2}{K_{pp}(s - \mathrm{j}\omega_1) + K_{ip}} + 1\right) \tag{31}$$

From (31), Z'_{pni} behaves as a negative resistance at the fundamental frequency i.e., Z'_{pni}=-1/$\boldsymbol{I}_{rdq1}$ and behaves as a capacitance when the frequency increases. Equation (31) simplify the impedance from 50 Hz to 200 Hz, and fully characterizes the impedance of DFIG within the bandwidth of the symmetrical PLL. In addition, (31) can be utilized to calculate the cut-off frequency of the filter based on impedance reshaping control strategy in Section V.

V. Impedance Reshaping Control Strategy

A. *Design of the Phase Compensation Controller*

According to Section IV, the parallel impedance $\boldsymbol{Z}_{pni}$ will cause the DFIG system to exhibit capacitance and resonance with the inductive grid. The basic idea is to introduce a virtual impedance to counteract the feedforward matrix $\boldsymbol{G}_{pni}$ as shown in the red path of Fig. 10. Since the parallel impedance $\boldsymbol{Z}_{pni}$ dominates the impedance characteristic of DFIG within the bandwidth of the symmetrical PLL, Fig. 9 ignores the influence of $\boldsymbol{Z}_{pnu}$ and $\boldsymbol{Z}_0$ when designing the virtual impedance.

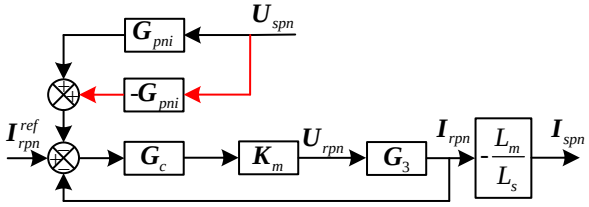

Fig. 10. Block diagram of DFIG impedance based on the virtual impedance.

It should be pointed that $\boldsymbol{U}_{spn}$ in Fig. 10 is the stator voltage in a system frame, which cannot be measured directly [23], it is more convenient to control the stator voltage in the controller frame. Therefore, Fig. 10 can be equivalently transformed into Fig. 11.

This article has been accepted for publication in a future issue of this journal, but has not been fully edited. Content may change prior to final publication. Citation information: DOI 10.1109/TPEL.2020.2982946, IEEE Transactions on Power Electronics

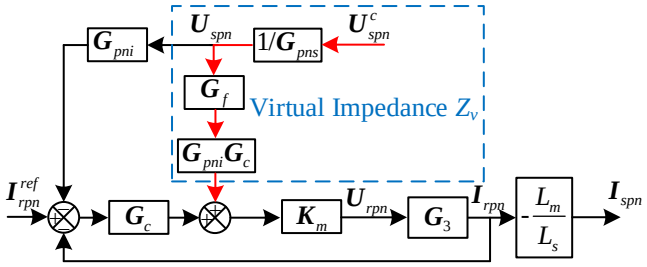

Fig. 11. Equivalent block diagram of DFIG impedance based on the virtual impedance.

In Fig. 11, $\boldsymbol{G}_f$ is the transfer matrix of filter which avoids to influence the DFIG impedance at 50 Hz, $\boldsymbol{G}_{pns}$ is the transfer matrix of stator voltage from controller frame to system frame, which can be written as,

$$\boldsymbol{G}_{pns}=\begin{bmatrix}1-U_{sd1}H_{PLL}(s) & 0\\ 0 & 1-U_{sd1}H_{PLL}(s)\end{bmatrix} \tag{32}$$

Therefore, the virtual impedance Z'_v can be written as,

$$\begin{aligned}Z'_v &\approx G'_f G'_{pni} G'_c / G'_{pns}\\ &= -\boldsymbol{I}_{rdq1}\frac{\left(K_{pp}(s-\mathrm{j}\omega_1)+K_{ip}\right)\left(K_{pc}(s-\mathrm{j}\omega_1)+K_{ic}\right)}{(s-\mathrm{j}\omega_1)^3}G'_f\end{aligned} \tag{33}$$

From (33), the phase compensation controller has three poles, which will influence the modulation output of the fundamental frequency, thus, a third-order high-pass filter should be introduced. Noted that the phase compensation controller in this paper can be equivalent to a low-pass filter because symmetrical PLL will lose the effect at high frequency, so the proposed virtual impedance will be a band-pass controller after adding a third-order high-pass filter.

The virtual impedance in this paper is in parallel with the rotor current controller, and the transfer function $\boldsymbol{G}_{ref}$ will remain unchanged after adding the paralleled virtual impedance [26]. Therefore, the proposed control strategy has no effect on the fundamental current, and rotor current control loop can achieve a zero steady for the rotor fundamental current.

B. Design of the High-pass Filter

The filter cut-off frequency can be obtained by (34), that is expressed based on the impedance expression (31) and the grid impedance expression sL_g. It is worth noting that as the SCR decreases, the DFIG system becomes more susceptible to resonance with the inductive weak grid. This paper considers SCR of 1.2 as extreme case to design the cut-off frequency of high-pass filter. Therefore, it is not necessary to modify the parameters of the proposed impedance reshaping control strategy when the power operation point and some control parameters changes.

$$-\frac{1}{\boldsymbol{I}_{rdq1}}\left(\frac{(s-\mathrm{j}\omega_1)^2}{K_{pp}(s-\mathrm{j}\omega_1)+K_{ip}}+1\right)=sL_g \tag{34}$$

Submitting the parameters of DFIG system in Table I and SCR of 1.2 into (34), the frequency of the intersection can be solved to be 60 Hz. So the cut-off frequency of high-pass filter should be less than 10 Hz to ensure the phase margin at the resonant frequency. Therefore, this paper chooses a third-order Butterworth high-pass filter with a cut-off frequency of 5Hz (ω_L=2π·5). The transfer function of filter G'_f can be expressed as,

$$G'_f=\frac{s^3}{s^3+2\omega_L s^2+2\omega_L{}^2 s+\omega_L{}^3} \tag{35}$$

Noted that although the impedance analysis in this paper is all in sequence-domain, the proposed virtual impedance can also be added in *dq*-domain like other controller based on the transformation matrix. The control diagram of the proposed impedance reshaping control strategy in *dq*-domain is shown as Fig.12.

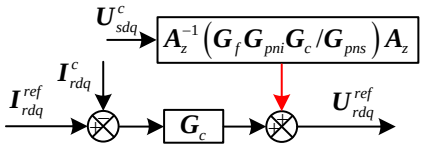

Fig. 12. Control diagram of the proposed impedance reshaping control strategy in *dq*-domain.

C. Analysis of the Virtual Impedance

Based on the above analysis, the impedance bode diagram of DFIG system with or without virtual impedance can be shown as in Fig. 13. Several conclusions can be reached as follows.

Firstly, the amplitude-frequency characteristic curve and phase-frequency characteristic curve within 47 Hz and 52 Hz are not changed after adding the virtual impedance because of the third-order high-pass filter. The phase of DFIG system starts to rise at 53 Hz, and the DFIG system behaves as a resistance from 150 Hz to 400 Hz, indicating a sufficient phase margin to avoid the resonance with the inductive grid. When the frequency is greater than 600 Hz, the virtual impedance gradually loses its effect, and that will not influence the high frequency phase.

Secondly, when the SCR of grid is 2, the intersection of amplitude-frequency characteristic curve moves from 136 Hz to 145 Hz after adding the virtual impedance. The difference of phase decreases from 181 ° to 90 °, which will eliminate the resonance problem due to the sufficient phase margin.

Thirdly, when the SCR of the grid is 1.5 and 2.8, the amplitude-frequency characteristic curve of the DFIG system and the grid intersect at 106 Hz and 172 Hz before adding the virtual impedance, respectively. Even though the resonance frequency shifts due to the SCR changes, the DFIG system with impedance reshaping control strategy always has a large phase margin between 106 Hz and 172 Hz. It should be noted that the paralleling high-pass filter significantly reduces the magnitude of DFIG system at the cut-off frequency of 5 Hz. The amplitude-frequency characteristic curve of the DFIG system and the grid will intersect at 54 Hz and 58 Hz when the SCR=1.5. However, since the phase difference between these two intersections is always greater than 180 ° as shown in Fig. 13, they will not cause stability problems according to the Nyquist criterion [17], because the trajectory of Nyquist diagram just passes through the unit circle first, and then out of the unit circle, rather than surround (-1,0). The detailed analysis has been studied in [17], and will not explain this problem again due to

This article has been accepted for publication in a future issue of this journal, but has not been fully edited. Content may change prior to final publication. Citation information: DOI 10.1109/TPEL.2020.2982946, IEEE Transactions on Power Electronics

the limited pages.

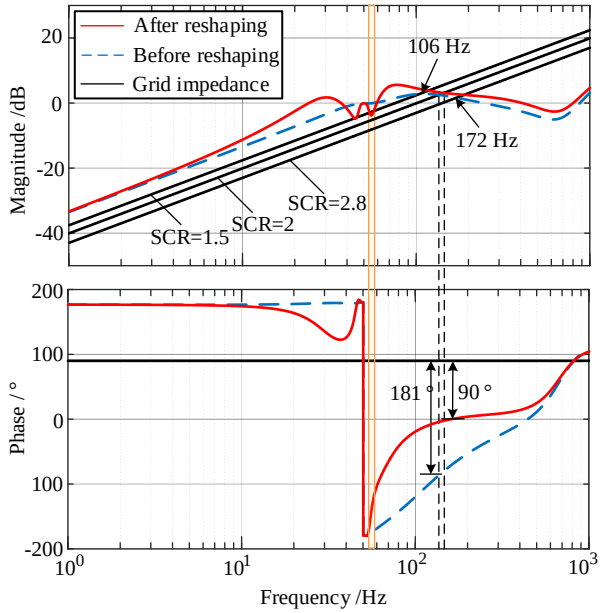

Fig. 13. Impedance Bode diagram of DFIG system with virtual impedance.

D. Robustness against DFIG Parameter Deviations

Practically, the parameters of DFIG are not constant due to the saturation, temperature change, and so on. And the DFIG system may switch to different operation conditions such as super synchronous conditions or sub synchronous conditions [27]. Therefore, it is necessary to analyse the robustness against DFIG parameter or operation conditions deviations.

The stator resistance and rotor resistance of the DFIG in this paper are very small, so the change of the resistance has little effect on the impedance characteristics of the DFIG. Fig .14 and Fig. 15 show the impedance Bode diagram of DFIG system with leakage inductance and rotor frequency variations. It can be seen that when the leakage inductance increases, the amplitude of the DFIG impedance at the frequency greater than 400Hz and the phase of the DFIG impedance at the frequency greater than 200Hz increases. When the rotor frequency decreases, the amplitude of the DFIG impedance at the frequency less than 30 Hz increases, and the phase of the DFIG impedance at the frequency less than 40Hz decreases. However, the DFIG system with the proposed impedance reshaping control strategy still keeps a high phase margin after the DFIG parameters change. Therefore, the proposed control strategy has an excellent robustness for the changed DFIG parameters or operation conditions.

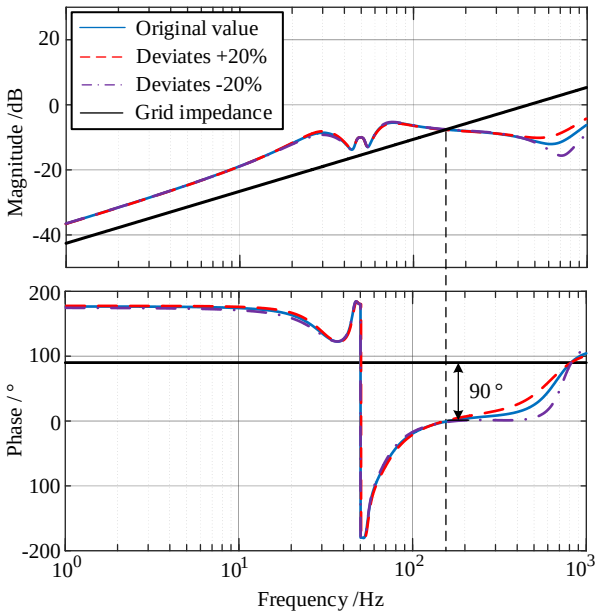

Fig. 14. Impedance Bode diagram of DFIG system with leakage inductance deviations.

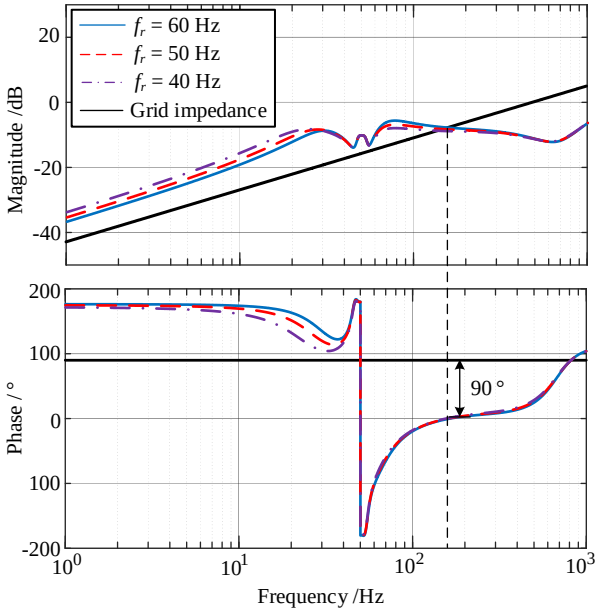

Fig. 15. Impedance Bode diagram of DFIG system with rotor frequency deviations

VI. Experimental Results

To futher verify the correctness of the proposed impedance reshaping method, the experiments based on Control-hardware-in-loop (CHIL) are carried out. The hardware platform of CHIL experiment is shown in Fig. 16. The model of DFIG is developed in Typhoon 602+ with the time step of 1 μs. Controllers of DFIG are implemented in a TMS320F28335 DSP+FPGA control board and the sampling frequency is set at 5 kHz. The parameters of DFIG are the same as the simulations, which are listed in Table I.

This article has been accepted for publication in a future issue of this journal, but has not been fully edited. Content may change prior to final publication. Citation information: DOI 10.1109/TPEL.2020.2982946, IEEE Transactions on Power Electronics

Fig. 16. Hardware platform of CHIL experiment.

In order to verify the impact of bandwidth of the symmetrical PLL and validate the feasibility of the proposed impedance reshaping control strategy, Fig. 17 shows the experimental results of DFIG system with or without proposed control strategy when the SCR is 2. The rotor speed is fixed at 1800 r/min. The reference output active and reactive power of DFIG system is 1.5 MW and 0 Var. The experimental results indicate that the DFIG system will be unstable after the bandwidth of the symmetrical PLL increases from 80 Hz to 140 Hz. The resonant frequency of the DFIG-grid interconnected system is 136 Hz which is the same as the analysis results in Fig. 6. The total harmonic distortion (THD) of the stator voltage U_{sabc} and current I_{sabc} are 6.3% and 5.4% according to FFT analysis. It also can be found that there is no other coupled resonant frequency, indicating that no frequency coupling characteristics in the DFIG system based symmetrical PLL. After enabling the proposed control strategy, the THD of stator voltage U_{sabc} and current I_{sabc} are reduced to 1.1% and 0.9%. The experimental results indicate that the proposed control strategy can improve the stability of the DFIG system when the bandwidth of the symmetrical PLL increases.

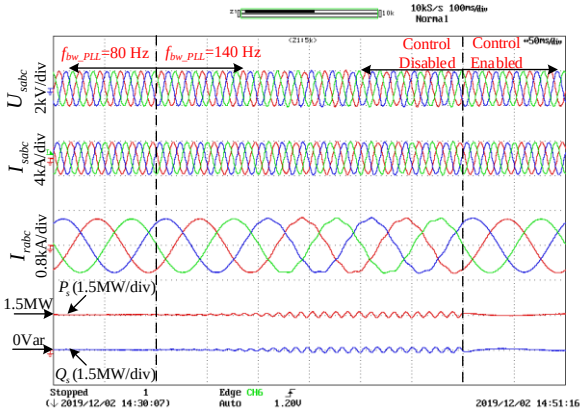

Fig. 17. Experimental results of DFIG system with proposed control strategy.

In order to verify the adaptability of the proposed impedance reshaping control strategy for resonance frequency shifts due to the SCR changes, Fig. 18 shows the experimental results of the DFIG system under inductive weak grid with the proposed control strategy, in which the SCR decreases from 2 to 1.5. The slight oscillations due to transient flux will occur after SCR decreases to 1.5, and the oscillations decay eventually because of the system damping. The experimental results indicate that the proposed control strategy can ensure a stable operation of DFIG system during the process of regulation, and still has good stability after SCR changes.

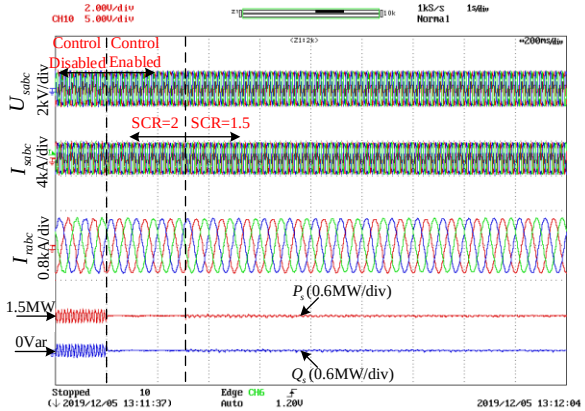

Fig. 18. Experimental results of adaptability of the proposed control strategy for resonance frequency shifts due to the SCR changes.

VII. Conclusions

This paper has analyzed the impedance characteristics of DFIG system based on symmetrical PLL. According the SISO impedance model and the block diagram of DFIG impedance subsystem, the coordinate transformation of rotor current will introduce a parallel impedance, which dominates the DFIG impedance characteristics within the bandwidth of the symmetrical PLL. An improved impedance reshaping control strategy is proposed to eliminate the resonance of DFIG-grid interconnected system when the bandwidth of symmetrical PLL increases. With the proposed control strategy, the DFIG system has an enough phase margin in the large frequency range when the resonance frequency shifts due to the SCR changes, without affecting the fundamental frequency control performance.

References

[1] S. Muller, M. Deicke and R. W. De Doncker, "Doubly fed induction generator systems for wind turbines," *IEEE Ind. Appl Mag*., vol. 8, no. 3, pp. 26-33, May/Jun. 2002.

[2] F. Blaabjerg, M. Liserre and K. Ma, "Power electronics converters for wind turbine systems," in *Proc. IEEE Energy Convers. Congr. Expo*., 2011, pp. 281-290.

[3] F. Blaabjerg and K. Ma, "Wind energy systems," in *Proceedings of the IEEE*, vol. 105, no. 11, pp. 2116-2131, Nov. 2017.

[4] I. Vieto, and J. Sun, "Sequence Impedance Modeling and Analysis of Type-III Wind Turbines", *IEEE Trans. Energy Convers.*, vol. 33, no. 2, pp. 537-545, Jun. 2018.

[5] Y. Song and F. Blaabjerg, "Analysis of middle frequency resonance in DFIG system considering phase locked loop," *IEEE Trans. Power Electron.*, vol. 33, no. 1, pp. 343–356, Jan. 2018.

[6] X. Xi, H. Geng, and Y. Geng, "Enhanced model of the doubly fed induction generator-based wind farm for small-signal stability studies of weak power system," *IET Renew. Power Gener.*, vol. 8, no. 7, pp. 765–774, Jul. 2014.

[7] J. Hu, Y. Huang, D. Wang, H. Yuan and X. Yuan, "Modeling of grid-connected DFIG-based wind turbines for DC-link voltage stability analysis," *IEEE Trans. Sustain. Energy.*, vol. 6, no. 4, pp. 1325-1336, Oct. 2015.

[8] W. Liu, X. Xie, X. Zhang and X. Li, "Frequency-coupling admittance modeling of converter-based wind turbine generators and the control-hardware-in-the-loop validation," *IEEE Trans. Energy Convers.*, vol. 35, no. 1, pp. 425-433, Mar. 2020.

[9] C. Zhang, X. Cai, M. Molinas and A. Rygg, "Frequency-domain modelling and stability analysis of a DFIG-based wind energy conversion

system under non-compensated AC grids: impedance modelling effects and consequences on stability," *IET Power Electron*., vol. 12, no. 4, pp. 907-914, Apr. 2019.

[10] K. Sun, W. Yao, J. Fang, X. Ai, J. Wen and S. Cheng, "Impedance modeling and stability analysis of grid-connected DFIG-based wind farm with a VSC-HVDC," *IEEE J. Emerg. Sel. Topics Power Electron*., to be published. doi: 10.1109/JESTPE.2019.2901747.

[11] Y. Xu, H. Nian, et al., "Frequency coupling characteristic modeling and stability analysis of doubly fed induction generator," *IEEE Trans. Energy Convers.*, vol. 33, no. 3, pp. 1475-1486, Sep, 2018.

[12] B. Wen, D. Boroyevich, R. Burogos, P. Mattavelli, and Z. Shen, "Analysis of D-Q small-signal impedance of grid-tied inverters," *IEEE Trans. Power Electron.*, vol. 31, no. 1, pp. 675–687, Jan. 2016.

[13] A. Rygg, M. Molinas, C. Zhang, and X. Cai, "A modified sequence domain impedance definition and its equivalence to the dq-domain impedance definition for the stability analysis of ac power electronic systems," *IEEE J. Emerg Sel. Topics Power Electron.*, vol. 4, no. 4, pp. 1383–1396, Dec. 2016.

[14] X. Wang, L. Harnefors and F. Blaabjerg, "Unified impedance model of grid-connected voltage-source converters", *IEEE Trans. Power Electron.*, vol. 33, no. 2, pp. 1775-1787, Feb, 2018.

[15] I. Vieto and J. Sun, "Refined small-signal sequence impedance models of type-III wind turbines," in *Proc. ECCE*, Portland, OR, USA, Sep. 2018, pp. 1-8.

[16] X. Wang, Y. W. Li, F. Blaabjerg and P. C. Loh, "Virtual-impedance-based control for voltage-source and current-source converters," *IEEE Trans. Power Electron.*, vol. 30, no. 12, pp. 7019-7037, Dec. 2015.

[17] D. Pan, X. Ruan, C. Bao, W. Li and X. Wang, "Optimized controller design for LCL-type grid-connected inverter to achieve high robustness against grid-impedance variation," *IEEE Trans. Ind. Electron*., vol. 62, no. 3, pp. 1537-1547, Mar. 2015.

[18] H. Liu, X. Xie, Y. Li, H. Liu and Y. Hu, "Mitigation of SSR by embedding subsynchronous notch filters into DFIG converter controllers," *IET Gener. Transmiss. Distrib*., vol. 11, no. 11, pp. 2888-2896, Sep. 2017.

[19] H. Nian and B. Pang, "Stability and power quality enhancement strategy for DFIG system connected to harmonic grid with parallel compensation," *IEEE Trans. Energy Convers.*, vol. 34, no. 2, pp. 1010-1022, Jun. 2019.

[20] X. Chen, Y. Zhang, S. Wang, J. Chen and C. Gong, "Impedance-phased dynamic control method for grid-connected inverters in a weak grid," *IEEE Trans. Power Electron.*, vol. 32, no. 1, pp. 274-283, Jan. 2017.

[21] S. Chou, X. Wang and F. Blaabjerg, "Two-port network modeling and stability analysis of grid-connected current-controlled VSCs," *IEEE Trans. Power Electron.*, doi: 10.1109/TPEL.2019.2934513.

[22] C. Zhang, X. Cai, A. Rygg and M. Molinas, "Sequence domain SISO equivalent models of a grid-tied voltage source converter system for small-signal stability analysis," *IEEE Trans. Energy Convers.*, vol. 33, no. 2, pp. 741-749, Jun. 2018.

[23] D. Yang, X. Wang, F. Liu, K. Xin, Y. Liu and F. Blaabjerg, "Symmetrical PLL for SISO impedance modeling and enhanced stability in weak Grids," *IEEE Trans. Power Electron.*, vol. 35, no. 2, pp. 1473-1483, Feb. 2020.

[24] C. Zhu, M. Hu and Z. Wu, "Parameters impact on the performance of a double-fed induction generator-based wind turbine for subsynchronous resonance control," *IET Renew. Power Gener*., vol. 6, no. 2, pp. 92-98, Mar. 2012.

[25] A. E. Leon, "Integration of DFIG-based wind farms into series-compensated transmission systems," *IEEE Trans. Sustain. Energy.*, vol. 7, no. 2, pp. 451-460, Apr. 2016.

[26] C. Wu and H. Nian, "Stator harmonic currents suppression for DFIG based on feed-forward regulator under distorted grid voltage," *IEEE Trans. Power Electron*., vol. 33, no. 2, pp. 1211-1224, Feb. 2018.

[27] B. Pang, H. Nian, C. Wu and P Cheng, "Stator harmonic currents suppression for DFIG system considering integer harmonics and interharmonics," *IEEE Trans. Ind. Electron*., vol. 66, no. 9, pp. 7001-7011, Sep. 2019.

Responses to editor's and reviewers' comments

The authors would like to appreciate the editor and reviewers for spending time reviewing our manuscript and providing valuable comments. We have carefully revised this manuscript and made amendments according to the specific changes posed by the reviewers. Changes are in red in the revised manuscript.

Reviewer: 1

Comments to the Author

This paper proposes a virtual impedance strategy based on symmetric phase-locked loop to improve the stability of DFIG under weak grid conditions. The author's answers to questions about voltage regulation speed and analysis of negative-sequence impedance stability are convincing. The logic of this article is reasonable after modification.

Author Response: Thanks for your comments.

Reviewer: 2

Comments to the Author

The Impedance characteristic of DFIG system based on symmetrical PLL is analyzed in this paper.

1. In Section Ⅲ. D, "keeps unchanged after transformation" is suggest to provide detailed derivation. The *dq*-domain and sequence-domain have frequency shift, hence are not same in *dq*-domain and sequence-domain.

Author Response: Thanks for your comments.

As the reviewer said, the *dq*-domain and sequence-domain have frequency shift of 50 Hz, which cannot be eliminated by the transformation matrix in equation (R1). It should be noted that the control matrices in the *dq* domain need to be shifted by 50 Hz in advance as shown in equation (R3), (R4), (R5), (R6) (corresponds to equation (10), (11), (12), (26) in this manuscript).

$$\boldsymbol{G}_{pn}=\boldsymbol{A}_z\boldsymbol{G}_{dq}\boldsymbol{A}_z^{-1} \tag{R1}$$

$$\boldsymbol{A}_z=\frac{1}{\sqrt{2}}\begin{bmatrix}1 & \mathrm{j}\\ 1 & -\mathrm{j}\end{bmatrix} \qquad \boldsymbol{A}_z^{-1}=\frac{1}{\sqrt{2}}\begin{bmatrix}1 & 1\\ -\mathrm{j} & \mathrm{j}\end{bmatrix} \tag{R2}$$

$$\Delta\boldsymbol{\theta}_{pll}=-\mathrm{j}\frac{H_p(s)}{s-\mathrm{j}\omega_1}\Delta\boldsymbol{U}_{sdq}^{c} \tag{R3}$$

$$H_p(s)=\frac{K_{pp}(s-\mathrm{j}\omega_1)+K_{ip}}{s-\mathrm{j}\omega_1} \tag{R4}$$

This article has been accepted for publication in a future issue of this journal, but has not been fully edited. Content may change prior to final publication. Citation information: DOI 10.1109/TPEL.2020.2982946, IEEE Transactions on Power Electronics

$$\Delta\boldsymbol{\theta}_{pll}=-\mathrm{j}H_{pll}(s)\Delta\boldsymbol{U}_{sdq}=-\mathrm{j}\frac{H_p(s)}{U_{sd1}H_p(s)+s-\mathrm{j}\omega_1}\Delta\boldsymbol{U}_{sdq} \tag{R5}$$

$$\boldsymbol{G}_c=\begin{bmatrix}\dfrac{K_{pc}(s-\mathrm{j}\omega_1)+K_{ic}}{s-\mathrm{j}\omega_1} & 0\\ 0 & \dfrac{K_{pc}(s-\mathrm{j}\omega_1)+K_{ic}}{s-\mathrm{j}\omega_1}\end{bmatrix} \tag{R6}$$

$\boldsymbol{G}_c$ is the rotor current controller matrix in *dq*-domain, K_{pc} and K_{ic} are the proportional and the integral gain of current controller. Noted that $\boldsymbol{G}_c$ keeps unchanged after transformation. The detailed derivation is shown as,

$$\begin{aligned}\boldsymbol{A}_z\boldsymbol{G}_c\boldsymbol{A}_z^{-1}&=\frac{1}{\sqrt{2}}\begin{bmatrix}1 & \mathrm{j}\\ 1 & -\mathrm{j}\end{bmatrix}\begin{bmatrix}\dfrac{K_{pc}(s-\mathrm{j}\omega_1)+K_{ic}}{s-\mathrm{j}\omega_1} & 0\\ 0 & \dfrac{K_{pc}(s-\mathrm{j}\omega_1)+K_{ic}}{s-\mathrm{j}\omega_1}\end{bmatrix}\frac{1}{\sqrt{2}}\begin{bmatrix}1 & 1\\ -\mathrm{j} & \mathrm{j}\end{bmatrix}\\ &=\frac{1}{2}\begin{bmatrix}\dfrac{K_{pc}(s-\mathrm{j}\omega_1)+K_{ic}}{s-\mathrm{j}\omega_1} & \mathrm{j}\dfrac{K_{pc}(s-\mathrm{j}\omega_1)+K_{ic}}{s-\mathrm{j}\omega_1}\\ \dfrac{K_{pc}(s-\mathrm{j}\omega_1)+K_{ic}}{s-\mathrm{j}\omega_1} & -\mathrm{j}\dfrac{K_{pc}(s-\mathrm{j}\omega_1)+K_{ic}}{s-\mathrm{j}\omega_1}\end{bmatrix}\begin{bmatrix}1 & 1\\ -\mathrm{j} & \mathrm{j}\end{bmatrix}\\ &=\frac{1}{2}\begin{bmatrix}\dfrac{K_{pc}(s-\mathrm{j}\omega_1)+K_{ic}}{s-\mathrm{j}\omega_1}+\dfrac{K_{pc}(s-\mathrm{j}\omega_1)+K_{ic}}{s-\mathrm{j}\omega_1} & \dfrac{K_{pc}(s-\mathrm{j}\omega_1)+K_{ic}}{s-\mathrm{j}\omega_1}-\dfrac{K_{pc}(s-\mathrm{j}\omega_1)+K_{ic}}{s-\mathrm{j}\omega_1}\\ \dfrac{K_{pc}(s-\mathrm{j}\omega_1)+K_{ic}}{s-\mathrm{j}\omega_1}-\dfrac{K_{pc}(s-\mathrm{j}\omega_1)+K_{ic}}{s-\mathrm{j}\omega_1} & \dfrac{K_{pc}(s-\mathrm{j}\omega_1)+K_{ic}}{s-\mathrm{j}\omega_1}+\dfrac{K_{pc}(s-\mathrm{j}\omega_1)+K_{ic}}{s-\mathrm{j}\omega_1}\end{bmatrix}\\ &=\begin{bmatrix}\dfrac{K_{pc}(s-\mathrm{j}\omega_1)+K_{ic}}{s-\mathrm{j}\omega_1} & 0\\ 0 & \dfrac{K_{pc}(s-\mathrm{j}\omega_1)+K_{ic}}{s-\mathrm{j}\omega_1}\end{bmatrix}\end{aligned} \tag{R7}$$

It can be found that $\boldsymbol{G}_c=\boldsymbol{A}_z\boldsymbol{G}_c\boldsymbol{A}_z^{-1}$, so the rotor current controller has the same form in *dq*-domain and sequence-domain. In addition, if the 2x2 matrix has the same diagonal elements and off- diagonal elements are 0, this 2x2 matrix will keep the same after transformation.

Author action: The control matrix in the *dq* domain has been shifted by 50 Hz in advance as shown in equation (10), (11), (12) in the manuscript.

2. There is no frequency coupling through symmetrical PLL, then the impedance magnitude of the off-diagonal elements should be much smaller than the diagonal elements， which is different from the conclusion in Fig. 4.

Author Response: Thanks for your comments. If the magnitude of the off-diagonal elements in Bode diagram of DFIG impedance is high, the frequency coupling characteristic can be ignored.

This article has been accepted for publication in a future issue of this journal, but has not been fully edited. Content may change prior to final publication. Citation information: DOI 10.1109/TPEL.2020.2982946, IEEE Transactions on Power Electronics

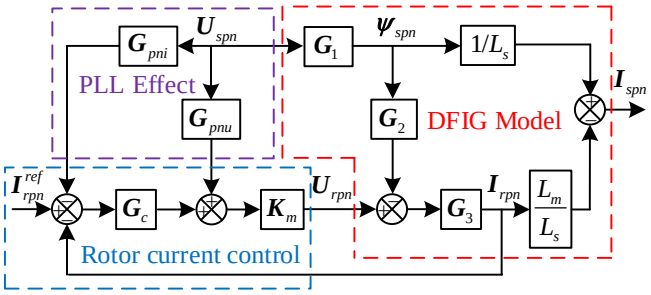

Fig. R1. DFIG impedance model based on symmetrical PLL.

According to Fig. R1, the stator current and the DFIG system admittance based on the symmetrical PLL can be expressed as,

$$\boldsymbol{I}_{spn} = \boldsymbol{Y}_{\mathrm{DFIG}} \boldsymbol{U}_{spn} + \boldsymbol{I}_{rpn}^{ref} \boldsymbol{G}_{ref} \tag{R8}$$

$$\boldsymbol{Y}_{\mathrm{DFIG}} = \begin{bmatrix} Y_{11} & 0 \\ 0 & Y_{22} \end{bmatrix} = \frac{1}{L_s}\boldsymbol{G}_1 - \left(\boldsymbol{I} + \boldsymbol{K}_m \boldsymbol{G}_c \boldsymbol{G}_3\right)^{-1} \frac{L_m}{L_s} \boldsymbol{G}_3 \left(\boldsymbol{K}_m \boldsymbol{G}_{pnu} - \boldsymbol{K}_m \boldsymbol{G}_c \boldsymbol{G}_{pni} - \boldsymbol{G}_2 \boldsymbol{G}_1\right) \tag{R9}$$

The Bode diagram of DFIG impedance can describe the impedance characteristics more intuitively, i.e., the DFIG behaves as an inductance when the DFIG phase is 90 °, or the DFIG behaves as a capacitance when the DFIG phase is -90 °. Therefore, this paper depicts the Bode diagram of DFIG impedance rather than DFIG admittance as shown in Fig. R2 (corresponds to Fig. 4 in this manuscript).

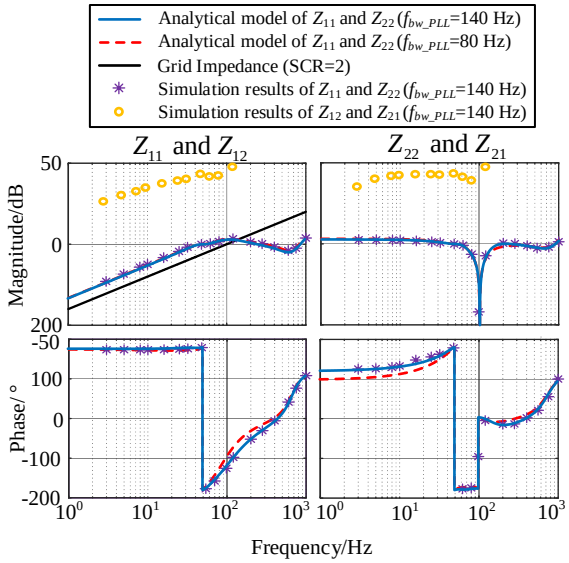

Fig. R2. Validation of DFIG impedance models based on symmetrical PLL.

If the impedance magnitude of the off-diagonal elements is high, the positive-sequence and negative-sequence will not affect each other due to a strong damping. Therefore, by comparing the diagonal elements Z_{11} and Z_{22} with the off-diagonal elements Z_{12} and Z_{21}, it can be seen that the magnitude of diagonal elements is much smaller than the off-diagonal elements, which means the frequency coupling characteristics can be neglected.

Author action: The reason why depicts the Bode diagram of DFIG impedance rather than DFIG admittance is added in the Section IV. A. The reason why the frequency coupling characteristics can be neglected when the impedance magnitude of the off-diagonal elements is high is added in the Section IV. A.

Reviewer: 3

Comments to the Author

An active damping control strategy is proposed for impedance shaping to eliminate resonance. It has good research significance for improving the stability of the DFIG system.

Author Response: Thanks for your comments.